

Reflection of audio sounds generated by a parametric array loudspeaker

Jiaxin Zhong,^{a)} Shuping Wang,^{b)} Ray Kirby,^{c)} and Xiaojun Qiu^{d)}

Centre for Audio, Acoustics, and Vibration, Engineering and Information Technology, University of Technology Sydney, New South Wales 2007, Australia

ABSTRACT:

The reflection of audio sounds generated by a parametric array loudspeaker (PAL) is investigated in this paper. The image source method and the non-paraxial PAL radiation model under the quasilinear approximation are used to calculate the reflected audio sound from an infinitely large surface with an arbitrary incident angle. The effects of the surface absorption in the ultrasound frequency range are studied, and the simulation and experiment results show that the reflection behavior of audio sounds generated by a PAL is different from those generated by traditional audio sources. The reason is that the reflected sound generated by the PAL consists of the reflection of audio sounds generated by incident ultrasounds and the audio sounds generated by the reflected ultrasound, and it is the latter that determines the directivity of the reflected audio sound. © 2020 Acoustical Society of America.

<https://doi.org/10.1121/10.0002161>

(Received 13 May 2020; revised 17 September 2020; accepted 18 September 2020; published online 26 October 2020)

[Editor: Mark Hamilton]

Pages: 2327–2336

I. INTRODUCTION

A parametric array loudspeaker (PAL) is an application of the parametric acoustic array for radiating highly directional audio sounds in air.^{1,2} Existing analytical models of the PAL consider the sound radiation in free space but do not pay much attention to its reflection, which is important in many applications.³ For example, PALs have been used to measure the sound absorption coefficients of materials in air^{4–6} and the reflection and transmission coefficients of elastomeric materials underwater,^{7,8} and actively control the binaural noise at human ears,⁹ where the reflection happens on the material surface or human skin and hair.

When a PAL radiates two intensive ultrasonic (primary) waves at different frequencies in a free field, secondary waves containing the difference-frequency wave (DFW; the audio sound in air) are generated due to the nonlinearity. The widely used model is based on the Khokhlov-Zabolotskaya-Kuznetsov (KZK) equation, which can be solved with many methods analytically or numerically; however, the results are usually only valid within the paraxial region, about 20° from the transducer axis.¹⁰ A non-paraxial model with better accuracy at wide angles was proposed recently under the quasilinear approximation,¹¹ which is extended in this paper to investigate the reflection of audio sounds generated by a PAL.

When there is a reflecting surface near a PAL, both primary and secondary sound waves are reflected by the

surface. The reflection by a pressure-release surface has been studied for underwater applications.¹² This model assumes that the primary fields are plane waves within the Rayleigh distance and spherical waves afterward, and the analysis is based on the weak shock wave theory. It was found that the DFW generated by the incident primary waves is antiphase with itself after the pressure-release reflection, while the DFW generated by the reflected primary waves is in-phase with the incident DFW. Therefore, the DFW suffers from a phase cancellation effect and this phenomenon has been observed in experiments.¹² The studies were then extended to the finite size planar targets with the weak nonlinearity by using a more accurate model.¹³

The reflection of the water-air (pressure-release) interface with a small grazing angle was modeled to investigate its effects on acoustic communication in shallow-water channels.¹⁴ Two theoretical models were proposed: a simplified Westervelt model in which the primary waves are highly attenuated within the collimated zone and a spherical spreading model in which the interaction of primary waves is significant in the far field spherically spreading beam. Experiments were conducted at 5.4° and 7.7° grazing angles, and only the spherical spreading model was shown to agree well with the experiment.

Except for the experimental studies conducted underwater in the aforementioned literature, the reflection of audio sounds generated by a PAL in air has also been studied experimentally.¹⁵ It was found that the sounds reflected from a rigid wall maintain the same directivity as the incident beam, but those reflected from a wall covered with a diffusive panel lose the directivity completely. However, the effects of the reflection of ultrasounds were not considered in this research. When a PAL radiates sound in air in the

^{a)}Electronic mail: Jiaxin.Zhong@student.uts.edu.au, ORCID: 0000-0002-9972-8004.

^{b)}ORCID: 0000-0002-0392-0246.

^{c)}ORCID: 0000-0002-3520-1377.

^{d)}ORCID: 0000-0002-5181-1220.

presence of a reflecting surface, additional audio sound components are generated by the reflected ultrasound waves. The two models proposed in Ref. 14 are only valid in the far field, whereas the model in Ref. 13 is valid in the near-field but limited to the paraxial region. The non-paraxial model in Refs. 11 and 16 is more accurate at the wide-angle field but has not considered reflections. In this paper, the non-paraxial model is extended to investigate the reflection of audio sound generated by a PAL. Simulations are carried out for oblique incident sound first, and then the experimental results are presented to verify the findings.

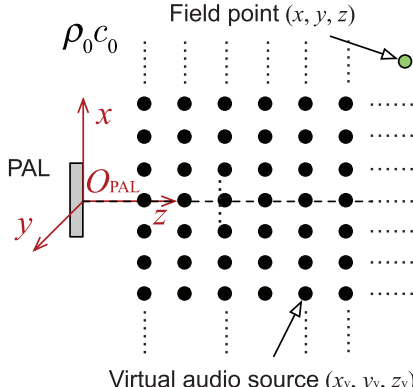
II. THEORY

The Westervelt equation governing the sound propagation in a lossy media, considering the nonlinear effects, is^{16,17}

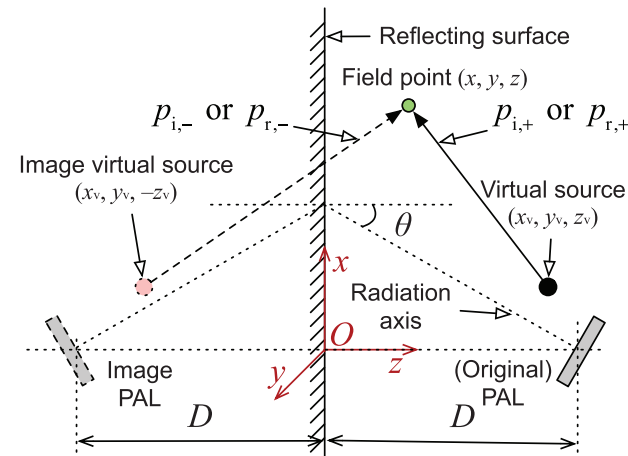
$$\nabla^2 p - \frac{1}{c_0^2} \frac{\partial^2 p}{\partial t^2} = - \frac{\delta}{c_0^4} \frac{\partial^3 p}{\partial t^3} - \frac{\beta}{\rho_0 c_0^4} \frac{\partial^2 p^2}{\partial t^2}, \quad (1)$$

where p is the sound pressure and c_0 is the linear sound speed. The first term on the right-hand side accounts for the fluid thermo-viscosity, where δ is the sound diffusivity parameter, which relates to the atmospheric sound attenuation coefficient α at the angular frequency ω by $\alpha(\omega) = \omega^2 \delta / (2c_0^3)$.^{18,19} The second term on the right-hand side accounts for the nonlinearity, where ρ_0 is the static fluid density and β is the nonlinearity coefficient. It is noteworthy that Eq. (1) cannot be used when the noncumulative (local) effects are predominant.^{20,21} Further simulations (not shown in this paper for conciseness) demonstrated that the error is less than 0.2 dB when the distance between the field point and the PAL is larger than 0.3 m for the parameters used in this paper, which indicates that Eq. (1) is sufficiently accurate for the model investigated.

As shown in Fig. 1(a), assume a PAL in free field generates two harmonic ultrasounds at frequencies f_1 and f_2



(a)



(b)

FIG. 1. (Color online) A PAL radiating sounds (a) in free field or (b) to an infinitely large reflecting surface with an incident angle θ .

($f_1 > f_2$) with the boundary condition on the transducer surface being

$$v_z(x, y, t) = v_1(x, y)e^{-j\omega_1 t} + v_2(x, y)e^{-j\omega_2 t}, \quad (2)$$

where j is the complex unit, v_z represents the vibration velocity normal to the transducer surface, v_n is the amplitude of the vibration velocity, $n = 1, 2$, $\omega_n = 2\pi f_n$ is the angular frequency of the n th primary wave, (x, y) is the transverse coordinate, and the z axis is perpendicular to the transducer surface under the coordinate system $O_{\text{PAL}}-xyz$. The solutions of the ultrasound and audio sound are denoted as

$$\tilde{p}_n(\mathbf{r}, t) = p_n(\mathbf{r})e^{-j\omega_n t}, \quad n = 1, 2, a, \quad (3)$$

where the subscripts 1, 2, and a represent the two ultrasounds and the audio sound, respectively, and $\mathbf{r} = (x, y, z)$ represents the spatial coordinates.

Because the ultrasound level generated by a PAL is limited for safety concerns, the nonlinearity is not very strong and the quasilinear approximation can be used in the derivation.² Assume that the sound pressure p in Eq. (1) consists of a primary sound pressure satisfying the linear and homogeneous version of Eq. (1) and a secondary sound pressure resulting from the source term.¹¹ After applying the successive method to Eq. (1), the sound pressure of the ultrasounds can be expressed as^{11,22}

$$p_n(\mathbf{r}) = -\frac{j\rho_0\omega_n}{2\pi} \iint_S v_n(x_s, y_s) \frac{e^{jk_nd_s}}{d_s} dx_s dy_s, \quad (4)$$

where S is the radiation surface, the wavenumber $k_n = \omega_n/c_0 + j\alpha_n$, with $n = 1$ and 2, and $d_s = \sqrt{(x - x_s)^2 + (y - y_s)^2 + z^2}$ is the distance between field point $\mathbf{r} = (x, y, z)$ and the source point $(x_s, y_s, 0)$ on the transducer surface. The audio sound can be treated as the contribution of the radiation by infinitely many virtual sources at $\mathbf{r}_v = (x_v, y_v, z_v)$, which has the source density function of²²

$$q(\mathbf{r}_v) = -\frac{j\beta\omega_a}{\rho_0^2 c_0^4} p_1(\mathbf{r}_v) p_2^*(\mathbf{r}_v). \quad (5)$$

The audio sound is then expressed as^{11,22}

$$p_a(\mathbf{r}) = -\frac{j\rho_0\omega_a}{4\pi} \int_0^\infty \int_{-\infty}^\infty \int_{-\infty}^\infty q(\mathbf{r}_v) \frac{e^{jk_a d_v}}{d_v} dx_v dy_v dz_v, \quad (6)$$

where the wavenumber $k_a = \omega_a/c_0 + j\alpha_a$, and $d_v = \sqrt{(x - x_v)^2 + (y - y_v)^2 + (z - z_v)^2}$ is the distance between field point \mathbf{r} and virtual source point \mathbf{r}_v , respectively. The ultrasound fields can be calculated by substituting Eq. (2) into Eq. (4), and then the audio field can be obtained from Eq. (6).

Figure 1(b) shows a PAL radiating ultrasounds to an infinitely large reflecting surface with an incident angle θ , where the distance between the PAL center and the reflecting surface is D , and the origin of the coordinate system, O , is set at the projection point of the PAL on the reflecting surface with the positive z axis pointing to the center of the PAL. When the sound beams impinge on the reflecting surface, both ultrasounds and audio sounds are reflected. The total audio sound mainly consists of four components as shown in Fig. 1(b), and can be expressed as

$$p_{a,t}(\mathbf{r}) = p_{i,+}(\mathbf{r}) + p_{i,-}(\mathbf{r}) + p_{r,+}(\mathbf{r}) + p_{r,-}(\mathbf{r}), \quad (7)$$

where $p_{i,+}$ is generated by the nonlinear interactions of incident ultrasounds, $p_{i,-}$ is the reflection of $p_{i,+}$ to satisfy the boundary condition on the reflecting surface for audio sounds, $p_{r,+}$ is generated by the nonlinear interactions of reflected ultrasounds, and $p_{r,-}$ is the reflection of $p_{r,+}$. These four components will be analyzed individually in the following. It is noteworthy that the nonlinear interactions of the incident and reflected ultrasound are neglected because of the phase mismatching of the ultrasound waves and small source density of the virtual source. Further simulations (not presented in this paper) show the audio sound generated by them is at least 35 dB less than that calculated by Eq. (7) for the parameters used in this paper, so they can be safely neglected to simplify the model and focus on the reflection phenomenon.

The audio sound generated by the incident ultrasounds is

$$p_{i,+}(\mathbf{r}) = -\frac{j\rho_0\omega_a}{4\pi} \int_0^\infty \int_{-\infty}^\infty \int_{-\infty}^\infty q_i(\mathbf{r}_v) \frac{e^{jk_a d_{v,+}}}{d_{v,+}} dx_v dy_v dz_v, \quad (8)$$

where $d_{v,+} = \sqrt{(x - x_v)^2 + (y - y_v)^2 + (z - z_v)^2}$ is the distance between the field point and the virtual source point. The source density function of the virtual source at (x_v, y_v, z_v) is

$$q_i(\mathbf{r}_v) = -\frac{j\beta\omega_a}{\rho_0^2 c_0^4} p_{1,i}(\mathbf{r}_v) p_{2,i}^*(\mathbf{r}_v), \quad (9)$$

where incident ultrasounds $p_{1,i}$ and $p_{2,i}$ are generated by the original PAL in free field at frequencies f_1 and f_2 , respectively.

To satisfy the boundary condition on the reflecting surface for the audio sound $p_{i,+}$, the image of each virtual source at (x_v, y_v, z_v) is assumed to be at $(x_v, y_v, -z_v)$ with the source density function $R_v(\omega_a)q_i(\mathbf{r}_v)$. $R_v(\omega_a)$ is the spherical wave reflection coefficient at frequency f_a , and $R_v(\omega_a) = 1$ when the boundary is rigid. For an arbitrary impedance boundary, $R_v(\omega_a)$ depends on frequency, the source, and field point locations, as well as the incident angle and the admittance of the boundary.²³ The audio sound generated by the image virtual source is then obtained by

$$p_{i,-}(\mathbf{r}) = -\frac{j\rho_0\omega_a}{4\pi} \int_0^\infty \int_{-\infty}^\infty \int_{-\infty}^\infty R_v(\omega_a)q_i(\mathbf{r}_v) \times \frac{e^{jk_a d_{v,-}}}{d_{v,-}} dx_v dy_v dz_v, \quad (10)$$

where $d_{v,-} = \sqrt{(x - x_v)^2 + (y - y_v)^2 + (z + z_v)^2}$ is the distance between \mathbf{r} and the image virtual source at $(x_v, y_v, -z_v)$. It is noteworthy that the spherical wave reflection coefficient is difficult to measure in experiments. Because the audio beams generated by the PAL behave like plane waves,⁴ the plane wave reflection coefficient can be used in Eq. (10) for simplicity.

The reflected ultrasounds are assumed to be the ultrasounds generated by the same PAL at the position of its image position multiplied by a plane wave reflection coefficient $R(\omega_1)$ and $R(\omega_2)$ at frequencies f_1 and f_2 , respectively. The audio sound generated by the reflected ultrasounds is then

$$p_{r,+}(\mathbf{r}) = -\frac{j\rho_0\omega_a}{4\pi} \int_0^\infty \int_{-\infty}^\infty \int_{-\infty}^\infty R(\omega_1)R^*(\omega_2)q_m(\mathbf{r}_v) \times \frac{e^{jk_a d_{v,+}}}{d_{v,+}} dx_v dy_v dz_v, \quad (11)$$

where the source density function of the virtual source is

$$q_m(\mathbf{r}_v) = -\frac{j\beta\omega_a}{\rho_0^2 c_0^4} p_{1,m}(\mathbf{r}_v) p_{2,m}^*(\mathbf{r}_v), \quad (12)$$

and $p_{1,m}$ and $p_{2,m}$ are the sound pressures of the corresponding ultrasound generated by the image PAL in free field at frequencies f_1 and f_2 , respectively. Similarly, to satisfy the boundary condition on the reflecting surface for the audio sound, the reflection of $p_{r,+}$ is

$$p_{r,-}(\mathbf{r}) = -\frac{j\rho_0\omega_a}{4\pi} \int_0^\infty \int_{-\infty}^\infty \int_{-\infty}^\infty R(\omega_1)R^*(\omega_2) \times R_v(\omega_a)q_m(\mathbf{r}_v) \frac{e^{jk_a d_{v,-}}}{d_{v,-}} dx_v dy_v dz_v. \quad (13)$$

After substituting Eq. (2) into Eq. (4), the incident and reflected ultrasound fields can be calculated, and then the total audio field can be obtained with Eq. (7). All of the

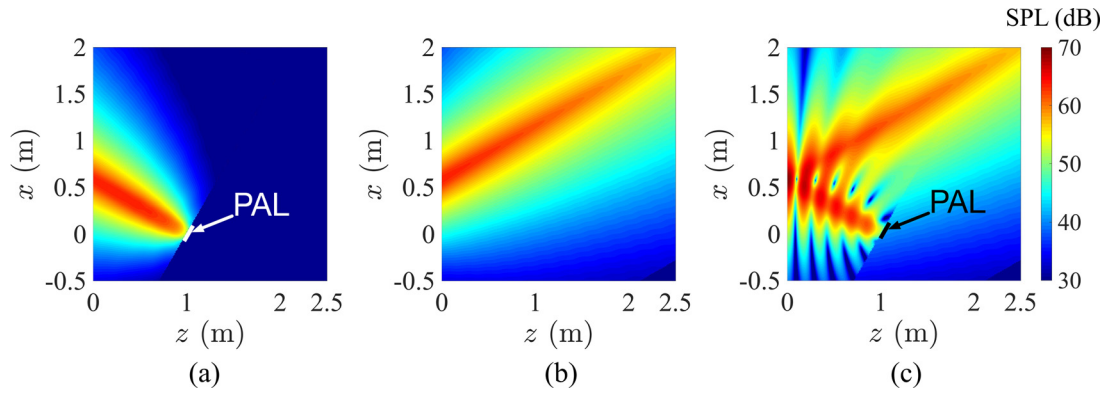


FIG. 2. (Color online) The audio sounds at 1 kHz generated by (a) the original PAL in free field, (b) the image PAL with respect to the reflecting surface, and (c) the PAL near a rigid reflecting surface.

integrals are calculated numerically without using the paraxial approximation, so the results are more accurate at low audio frequencies and wide angles.¹¹

III. SIMULATIONS AND DISCUSSIONS

In the following simulations, a circular piston with a radius of $a = 0.1$ m is considered, which is driven by a surface vibration velocity amplitude of 0.12 m/s. The sound pressure level (SPL) of ultrasounds at both frequencies is approximately 125 dB at 1 m away on the PAL radiation

axis when the PAL is placed in free field. The ultrasound frequencies are set as $f_1 = 61$ kHz and $f_2 = 60$ kHz, so the audio frequency is $f_a = 1$ kHz. The absorption coefficients of ultrasounds in air are 0.232 Neper/m and 0.228 Neper/m, respectively, which are calculated based on ISO 9613-1 at 20°C with the relative humidity being 50% and the ambient pressure being the standard atmospheric pressure.²⁴ The Rayleigh distance at 60 kHz is 5.5 m and the absorption length is 2.17 m.

To simplify the calculation, the infinitely large integral domain of the triple integral in Eq. (7) is reduced to a

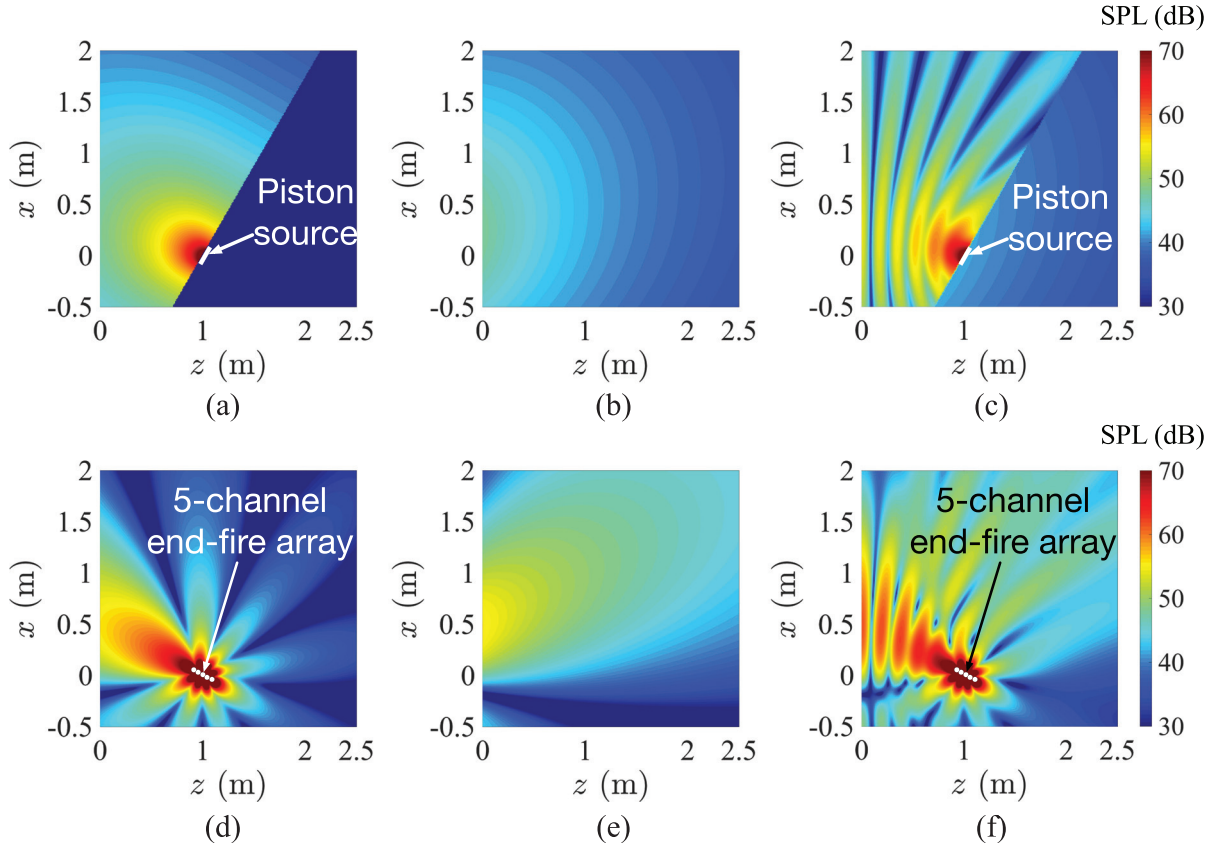


FIG. 3. (Color online) Sound fields at 1 kHz where (a), (b), and (c) are the incident, reflected, and total sounds radiated by a piston source, respectively, and (d), (e), and (f) are the incident, reflected, and total sounds radiated by a five-channel end-fire array, respectively.

specific region covering the major energy of ultrasound beams,¹⁶ and it has been confirmed that the error introduced by this reduction is smaller than 0.1 dB for the parameters used in this paper. Here, the integral domain is reduced to two truncated cylindrical columns with a radius of 3 m (30 times the PAL radius) and a length of 10 m (more than 4 times the effective absorption length) centered on the axis of the PAL and its image. The first column is for the calculation of the nonlinear interactions of incident ultrasounds, i.e., Eqs. (8) and (10), and starts from the PAL surface in the direction of the radiation axis and is terminated by the reflecting surface. The second column is for the calculation of the nonlinear interactions of reflected ultrasounds, i.e., Eqs. (11) and (13), and starts from the end of the first column in the direction of the axis of the image PAL. Only the ultrasound pressure inside the two columns is considered. All of the integrals are calculated numerically using the 1/3 Simpson's rule (Sec. 2.2 in Ref. 25).

Figure 2 shows the audio sounds generated by a PAL in free field (at 30° incidence) at its original and image source locations and the total audio sound field calculated by Eq. (7), where the reflecting surface is rigid for both ultrasounds and audio sound, and the distance to the PAL is $D = 1$ m. It

is clear that the total audio sound shown in Fig. 2(c) is the superposition of the other two shown in Figs. 2(a) and 2(b). The interference between the reflected and incident waves happens near the reflecting surface like two plane waves because the audio beams generated by the PAL behave like plane waves. The sound pressure on the back side ($z > D = 1$ m) focuses on the reflection axis and is almost equivalent to the sound radiated by the image PAL.

For comparison with traditional sources, the incident, reflected, and total sound radiated by an audio piston source and a traditional directional sound source are calculated and shown in Fig. 3 at 1 kHz. The piston source is the same size as the PAL and mounted on an infinitely large baffle, so the sound radiates only in the forward direction. The directional source is a compact end-fire array consisting of five point monopoles with an interval of 0.045 m as described in Ref. 26. By comparing Figs. 2 and 3, it can be found that the reflection for the audio sound generated by the PAL is much stronger than that generated by the other two traditional audio sound sources.

The mechanism of the reflected audio sounds generated by the PAL is different from that generated by traditional audio sources. It can be explained by analyzing the

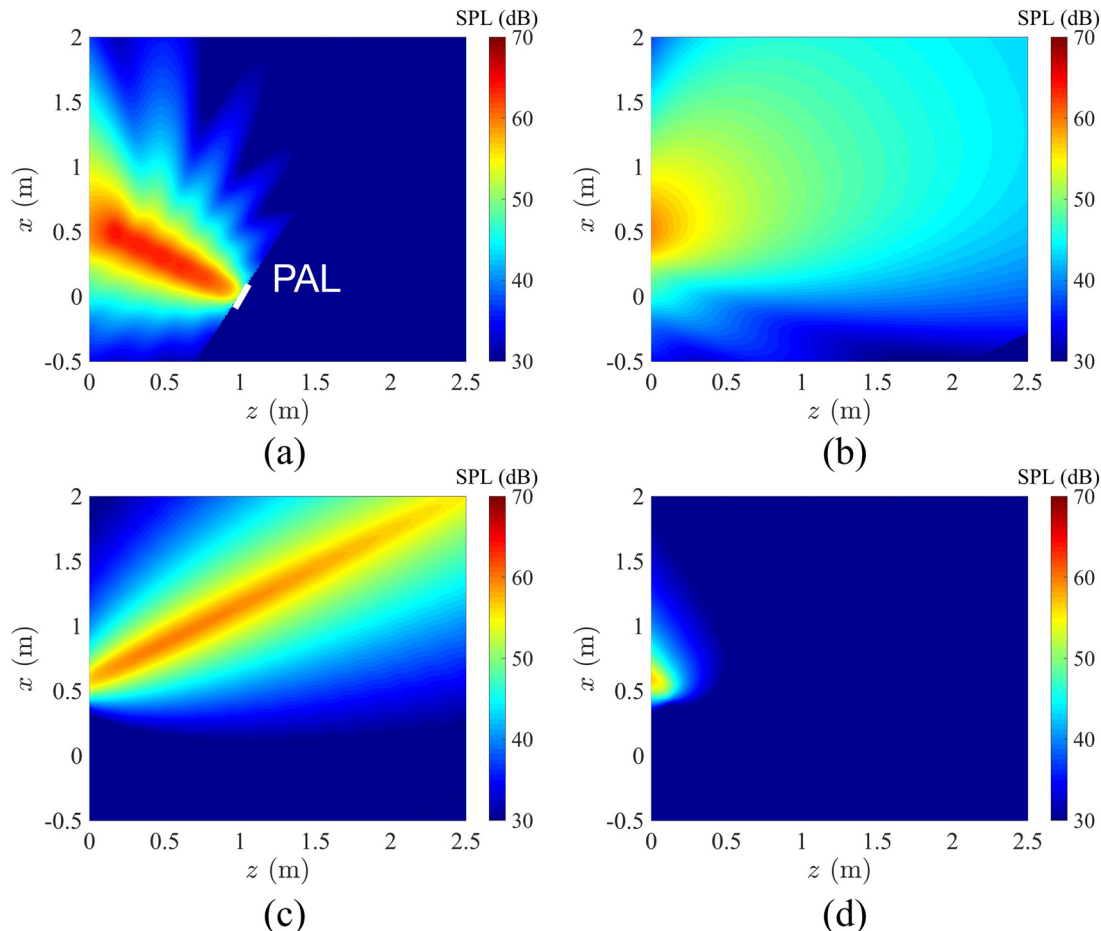


FIG. 4. (Color online) SPL distributions of four audio components radiated by the PAL at 30° incidence near a rigid reflecting surface with the distance of 1 m. (a) and (b) show the audio sounds generated by the incident ultrasounds and their reflections, respectively; (c) and (d) the audio sound generated by the reflected ultrasounds and their reflections, respectively.

four components in Eq. (7) for the PAL, and the calculated sound fields are shown in Fig. 4, using the same parameters in Fig. 2. The total sound pressure [shown in Fig. 2(c)] is the superposition of the audio sound generated by the incident ultrasounds [$p_{i,+}$, shown in Fig. 4(a)] and its reflection [$p_{i,-}$, shown in Fig. 4(b)], and the audio sound generated by the reflected ultrasounds [$p_{r,+}$, shown in Fig. 4(c)] and its reflection [$p_{r,-}$, shown in Fig. 4(d)]. The audio sound generated by the original PAL [shown in Fig. 2(a)] is the superposition of $p_{i,+}$ and $p_{r,-}$, and the one generated by the image PAL [shown in Fig. 2(b)] is the superposition of $p_{i,-}$ and $p_{r,+}$. It can be found that the audio sound generated by the reflected ultrasounds ($p_{r,+}$) is the dominant contributor to the directivity of the reflected audio sound of the PAL.

The amplitude of the audio sounds generated by reflected sounds is affected by the distance between the PAL and the reflecting surface (D). Figure 5 shows the audio sound field generated by the PAL at 30° incidence with the reflection surfaces at $D = 2$ m and 4 m. Compared with Fig. 2, the amplitude of the audio sounds generated by the reflected sounds becomes small as D increases. This is because the amplitude of the reflected ultrasounds becomes smaller when the PAL moves farther away from the reflecting surface, especially when the distance is larger than the effective absorption length (2.17 m, in this case).

In some applications, reflecting surfaces, such as thin carpets, can be highly absorbent for the ultrasounds but less

absorbent for the audio sounds. Figure 6 shows the audio sounds generated by the original PAL and its image, as well as the total sound fields when the sound absorption coefficient of the reflecting surface is 0.5 and 0.9 for ultrasounds ($1 - |R(\omega_1)R^*(\omega_2)|$), and 0 for audio sounds. Because the reflected ultrasound is small with a large sound absorption coefficient, the total sound pressure mainly consists of the audio sounds generated by the incident ultrasounds. The directivity of the reflected audio beams becomes worse for a larger ultrasound absorption coefficient of the reflecting surface.

Sound absorption in air is different at different frequencies, especially at high frequencies. Figure 7 shows the audio sounds of PAL at 30° incidence with reflection when $D = 1$ m. The ultrasound frequencies are 100 kHz and 101 kHz, or 200 kHz and 201 kHz. The absorption coefficients at 100 kHz (101 kHz) and 200 kHz (201 kHz) in air are 0.38 Neper/m and 0.95 Neper/m, respectively. The effective absorption lengths at 100 kHz (101 kHz) and 200 kHz (201 kHz) in free field are 1.32 m and 0.53 m, respectively. It can be found by comparing Fig. 7 with Fig. 2 that the amplitude of reflected audio beams decreases and the directivity deteriorates as the ultrasound frequency increases. All of the aforementioned analyses demonstrate that the reflection of audio sounds generated by a PAL differs from the traditional directional source because the properties of ultrasounds should be taken into account.

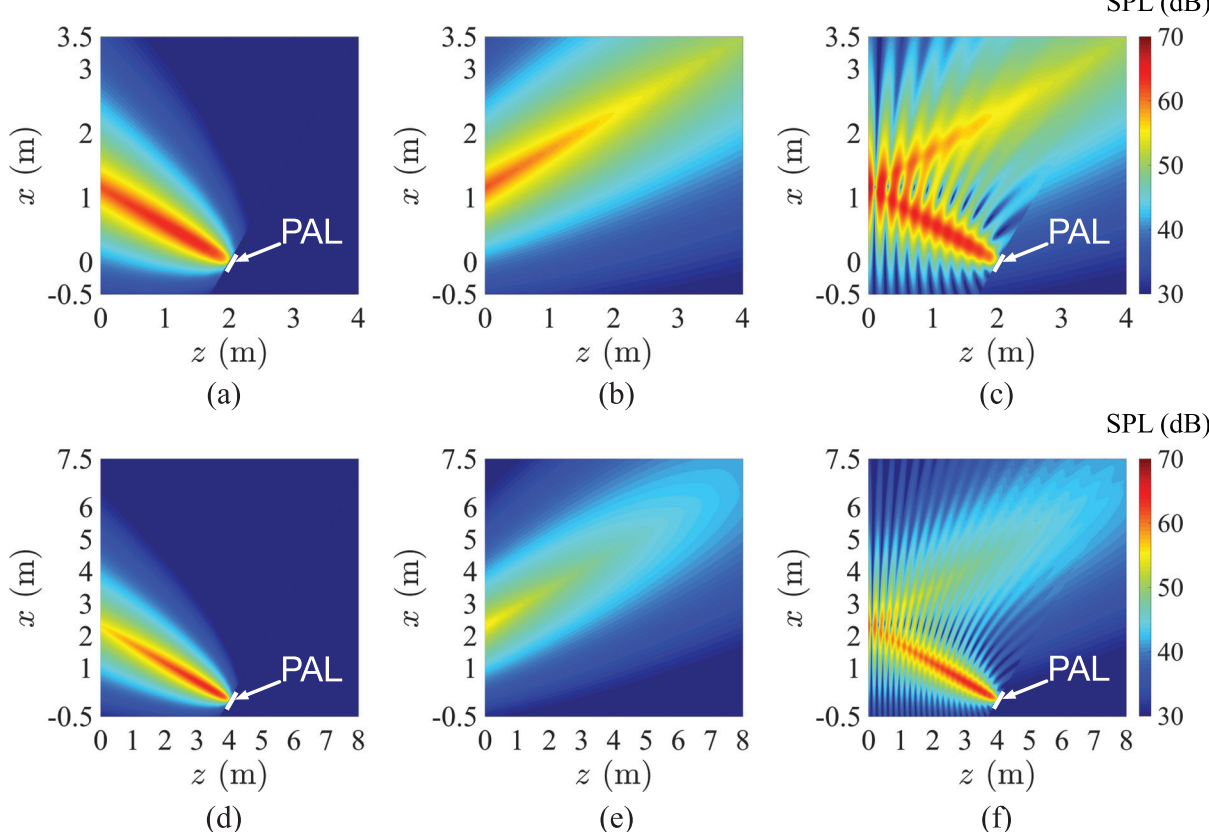


FIG. 5. (Color online) The audio sounds generated by the original PAL and the image PAL and the total fields with different distances between the PAL and the reflecting surface. (a)–(c) are for the distance of 2 m, and (d)–(f) are for the distance of 4 m.

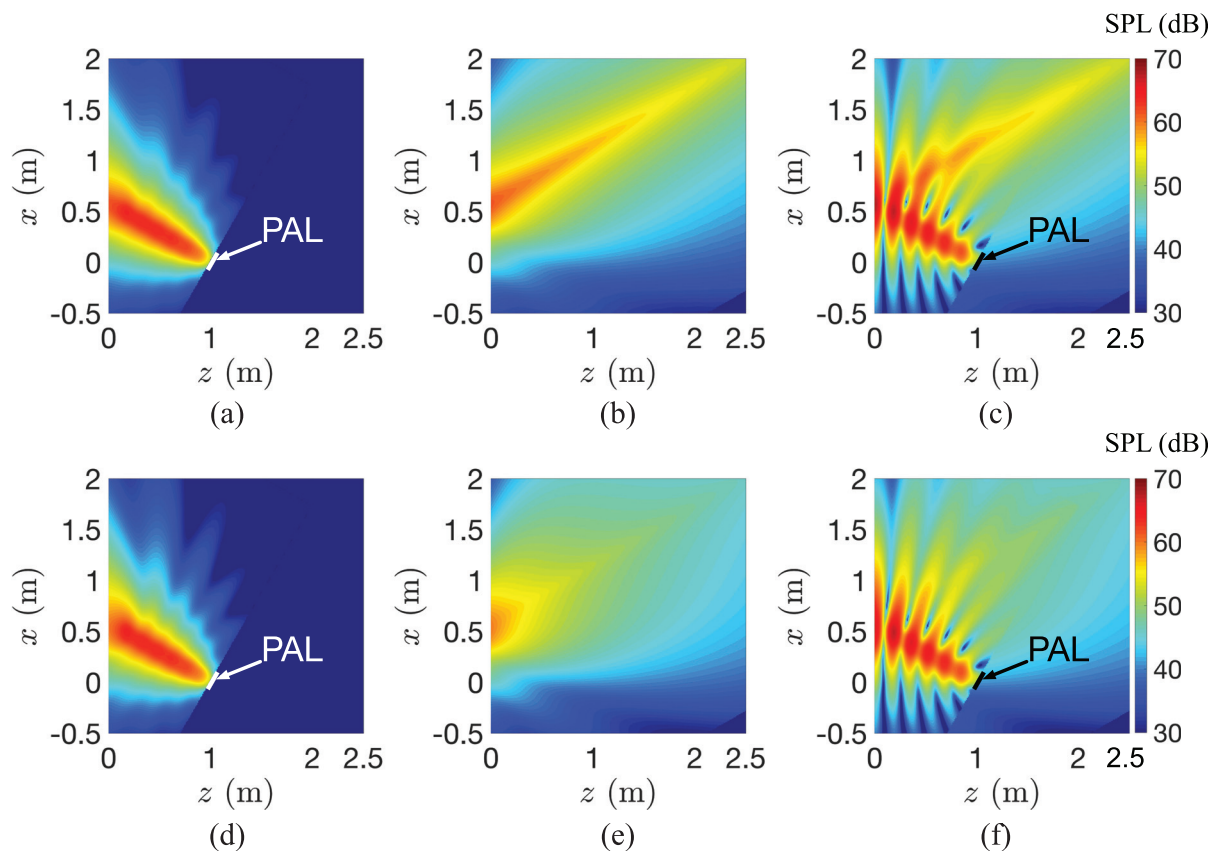


FIG. 6. (Color online) The audio sounds generated by the original PAL and its image and the total fields with different sound absorption coefficients of the reflecting surface. (a)–(c) are for ultrasound sound absorption coefficient of 0.5, and (d)–(f) are for ultrasound sound absorption coefficient of 0.9.

IV. EXPERIMENTS

Experiments were conducted in a hemi-anechoic room with dimensions of $7.20\text{ m} \times 5.19\text{ m} \times 6.77\text{ m}$ (height). A sketch and photos of the experimental setup are shown in Figs. 8 and 9, respectively. The sound field generated by a PAL, a traditional omnidirectional loudspeaker (point monopole), and a horn loudspeaker (directional source) with and without a cotton sheet on the ground were measured at 1 kHz. The preliminary test shows that the cotton sheet used in the experiments has a high absorption coefficient for ultrasonic sounds (more than 0.8) and a low absorption coefficient for audio sounds at 1 kHz (about 0.05).

Figure 8 shows a sketch of the experimental setup when the PAL radiates toward the ground. The sound field was measured at many points distributed on a vertical plane across the center of the testing loudspeaker. The length and height of the measurement plane are 3 m and 2.5 m, respectively. A custom made 60-channel microphone array with the microphone spacing of 5 cm was used to measure the sound pressure. The spacing between measurement points in the vertical direction is 5 cm when the microphone array is close to the loudspeaker and 10 cm in the other areas. All measurement microphones were Brüel and Kjær type 4957 microphones (Brüel and Kjær, Nærum, Denmark), and they were calibrated by a Brüel and Kjær type 4231 calibrator. The sound pressure was sampled with a Brüel and Kjær PULSE system (the analyzer 3053-B-120 with the input

panel UA-2107-120) and the fast Fourier transform (FFT) analyzer in PULSE LabShop (Brüel and Kjær, Nærum, Denmark) was used to obtain the FFT spectrum. The frequency span was set to 6.4 kHz with 6400 lines and the averaging type is linear with 66.67% overlap and 30 s duration.

The PAL, point monopole sound source 400 Pleasant St. Watertown, MAUSA, and traditional directional source used in the experiments are Holosonics Audio Spotlight AS-24i (Holosonics, Watertown, MA) with the surface sizes of $60\text{ cm} \times 60\text{ cm}$, a Genelec 8010A traditional voice coil loudspeaker, and a Daichi dome horn loudspeaker with a $24\text{ cm} \times 8\text{ cm}$ rectangular opening, respectively. The carrier frequency of the PAL is 64 kHz, according to measurements with a Brüel and Kjær type 4939 microphone (Brüel and Kjær, Nærum, Denmark), and the audio frequency in the experiments was set to 1 kHz. The radiating surface of the PAL is covered by a 6 mm thick perspex panel with a hole of radius 10 cm at its center to simulate the circular PAL used in simulations as shown in Fig. 9(a). To ensure the perspex panel is thick enough to block the audio sounds generated by the PAL, further experiment results (not presented here) show that the SPLs on the radiation axis of the PAL decrease by more than 30 dB at 1 kHz when the PAL is covered by a same size perspex panel without the hole. Therefore, a circular piston source was constructed using the 6 mm thick panel with a hole. To avoid spurious sounds at microphones induced by the intensive ultrasounds radiated by the PAL,²⁷ all the microphones were

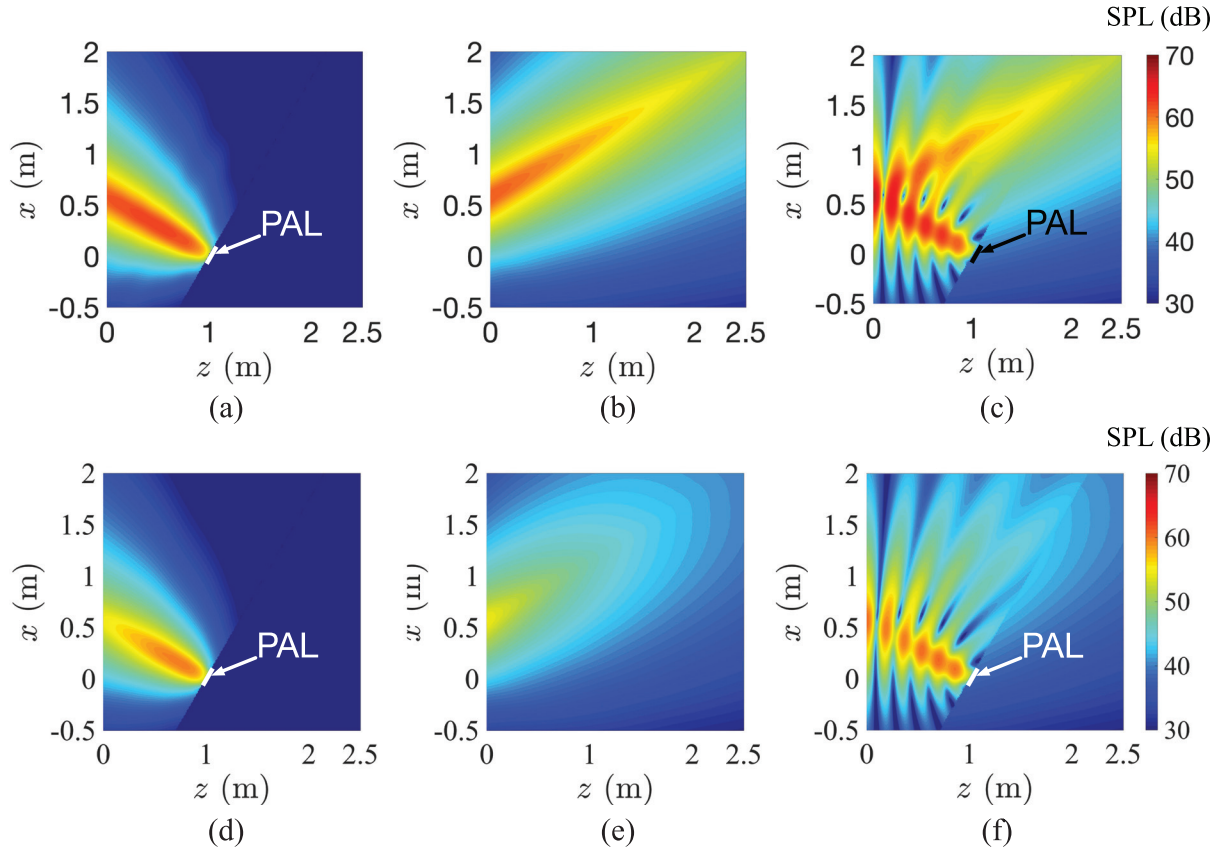


FIG. 7. (Color online) The audio sounds generated by the PAL, its image, and the total sound field at 30° incidence near a rigid reflecting surface with $D = 1$ m. (a)–(c) are for the ultrasounds frequencies of 100 kHz and 101 kHz, and (d)–(f) are for the ultrasounds frequencies of 200 kHz and 201 kHz.

covered by a piece of small and thin plastic film in the tests. The experimental results (not presented here) show the insertion loss of this plastic film is more than 35 dB at 64 kHz and less than 0.6 dB at 1 kHz. The relative humidity and the temperature in the experiments were 68% and 25.4°C , respectively.

A thin cotton sheet was used in the experiments to simulate a surface with high absorption for ultrasounds at 64 kHz but low absorption for audio sounds at 1 kHz. The thickness of the sheet is $250 \mu\text{m}$ and the surface density is 0.12 kg/m^2 . The size of the cotton sheet is $2.8 \text{ m} \times 4 \text{ m}$ and it is placed on the ground so that the projection of the center of the loudspeaker is on the bisector with respect to the narrower side (2.8 m) as shown in Fig. 8. The sound absorption coefficient of the cotton sheet was measured according to the two-microphone method specified in ISO 10534-2 (2001) using the Brüel and Kjær type

4206 impedance tube (Brüel and Kjær, Nærum, Denmark) and the value is 0.05 at 1 kHz,²⁸ so it has little effect on the audio sounds generated by the conventional loudspeakers.

Figure 10 shows the measured sound fields at 1 kHz generated by different loudspeakers at 30° incidence with and without the cotton sheet on the ground. Due to operation difficulties, the sound fields in the rectangular regions ($0.85 \text{ m} \leq z \leq 2.5 \text{ m}, -0.5 \text{ m} \leq x \leq 0.35 \text{ m}$), ($1 \text{ m} \leq z \leq 1.2 \text{ m}, -0.5 \text{ m} \leq x \leq 0.35 \text{ m}$), and ($0.9 \text{ m} \leq z \leq 1.3 \text{ m}, -0.5 \text{ m} \leq x \leq 0.35 \text{ m}$) were not measured for the three configurations, respectively, which are marked as blank regions in Fig. 10.

It can be seen in Fig. 10(a) that the reflected audio sounds are still highly focused on the axis in the reflection direction as expected, but they drop by up to 6 dB on the reflection axis with the cotton sheet placed on the ground as shown in Fig. 10(d). However, the reflected sounds generated by the traditional loudspeakers are almost the same with and without the cotton sheet. The results indicate that the reflected audio sounds generated by the PAL are not only the reflections of audio sounds generated by incident ultrasounds, but they also contain new audio sounds generated by reflected ultrasounds, and it is the latter that determines the directivity of the reflected audio sound.

V. CONCLUSIONS

In this paper, a non-paraxial PAL radiation model under the quasilinear approximation is extended to investigate the

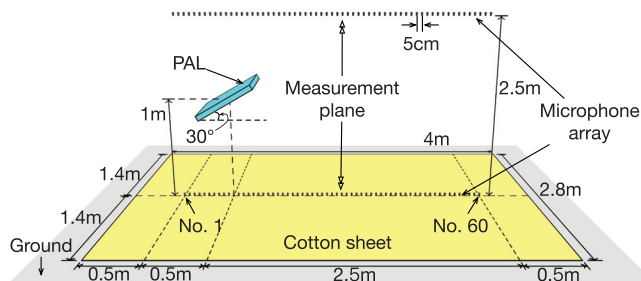


FIG. 8. (Color online) Sketch of the experimental setup when a PAL radiates toward the ground with and without a cotton sheet.

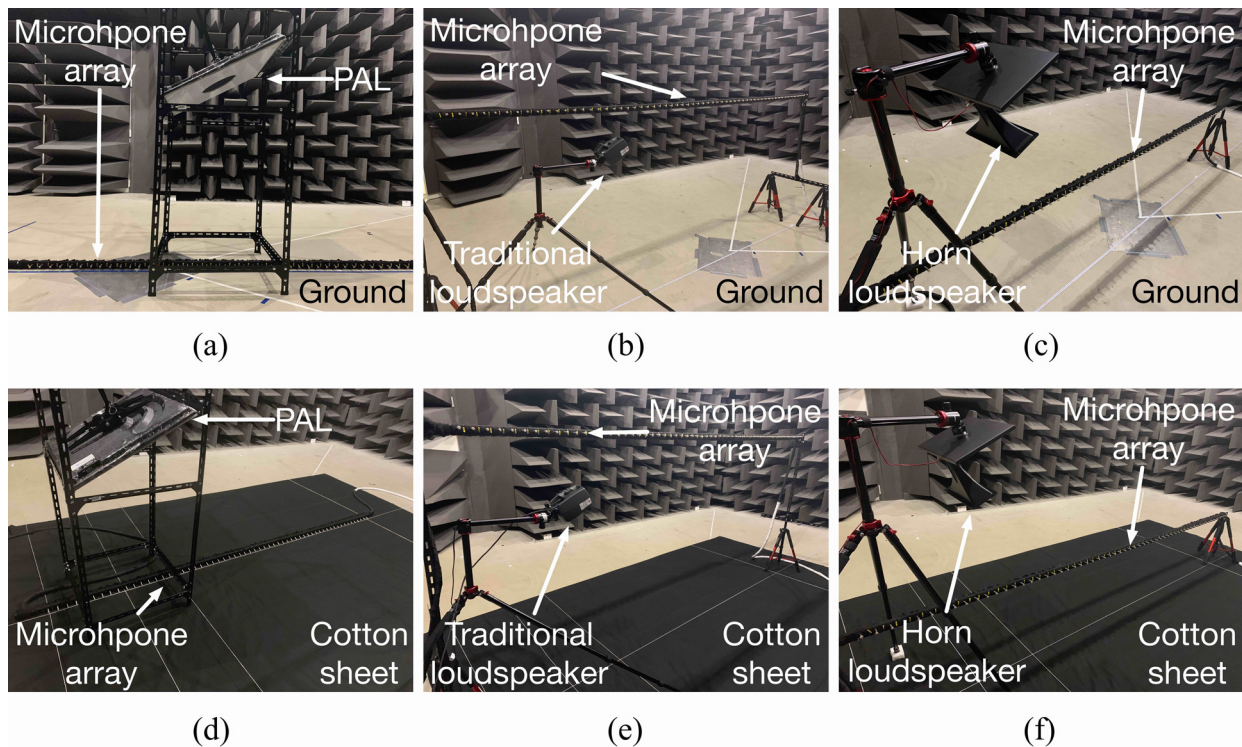


FIG. 9. (Color online) Photos of the experimental setups when different loudspeakers radiate toward the ground without the cotton sheet (a) the PAL, (b) the traditional omnidirectional loudspeaker, and (c) the horn loudspeaker, and with the cotton sheet (d) the PAL, (e) the traditional omnidirectional loudspeaker, and (f) the horn loudspeaker.

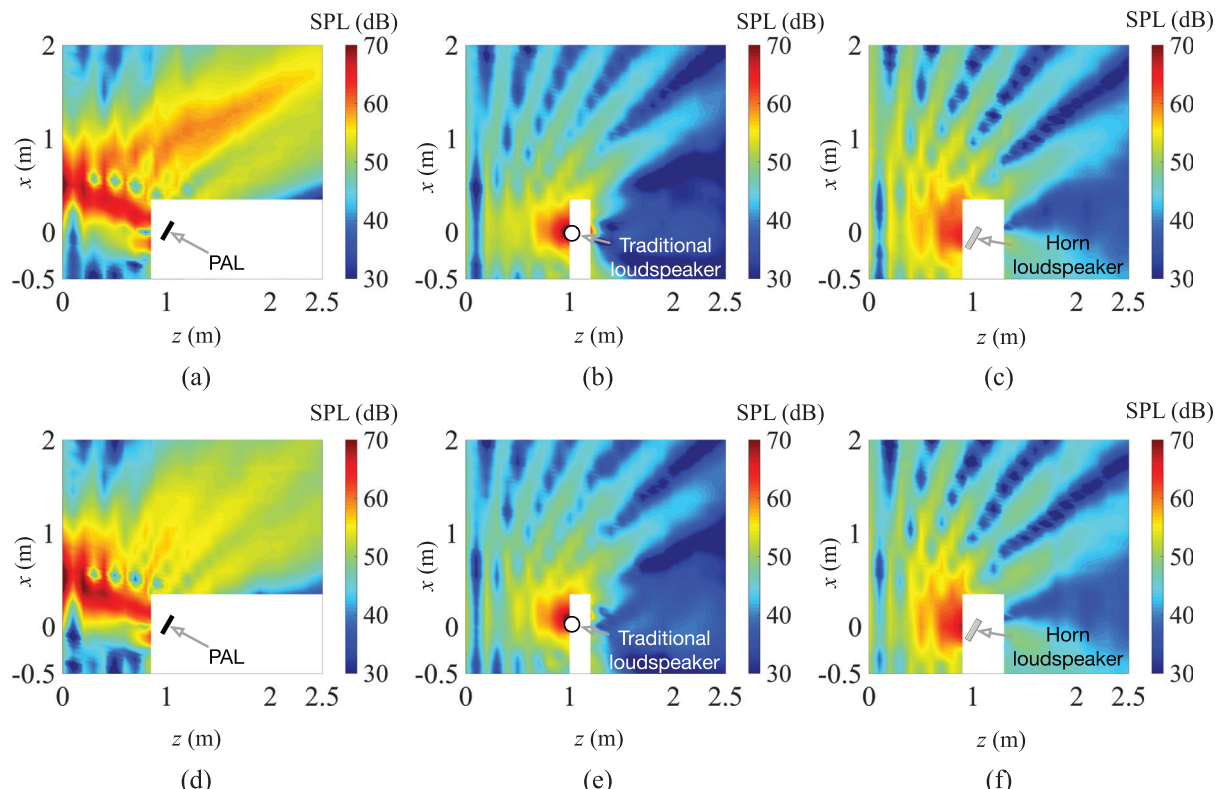


FIG. 10. (Color online) Measured sounds fields at 1 kHz generated by different loudspeakers at 30° incidence without the cotton sheet for (a) the PAL, (b) the traditional omnidirectional loudspeaker, and (c) a horn loudspeaker, and with the cotton sheet on the ground for (d) the PAL, (e) the traditional omnidirectional loudspeaker, and (f) a horn loudspeaker.

reflection of audio sounds in air generated by a PAL based on the image source method. It is shown that the reflected audio sound generated by a PAL contains not only the reflected audio sound but also the audio sound generated by the reflected ultrasound. This is different from the reflection with traditional audio sound sources. For a PAL, if the reflecting surface is highly absorbent for ultrasounds, the directivity of reflected audio sounds is no longer retained because the reflected ultrasounds are small. The experimental results show a thin cotton sheet with a thickness of 250 μm on a hard surface can absorb a large portion of the reflected audio sounds (up to about 6 dB on the reflection axis) generated by a PAL but has little effect on that generated by a traditional loudspeaker. Future work includes exploring the corrections in sound absorption coefficient measurements using PALs and measuring sound absorption coefficients of materials in the ultrasonic frequency range.

ACKNOWLEDGMENTS

This research is supported under the Australian Research Council's Linkage Project funding scheme (Grant No. LP160100616).

- ¹M. B. Bennett and D. T. Blackstock, "Parametric array in air," *J. Acoust. Soc. Am.* **57**(3), 562–568 (1975).
²W. S. Gan, J. Yang, and T. Kamakura, "A review of parametric acoustic array in air," *Appl. Acoust.* **73**(12), 1211–1219 (2012).
³Holosonic Research Labs, "User's Manual of Audio Spotlight," (Holosonic Research Labs, Watertown, MA, 2016).
⁴B. Castagnède, A. Moussatov, D. Lafarge, and M. Saeid, "Low frequency *in situ* metrology of absorption and dispersion of sound absorbing porous materials based on high power ultrasonic non-linearly demodulated waves," *Appl. Acoust.* **69**(7), 634–648 (2008).
⁵A. Sugahara, H. Lee, S. Sakamoto, and S. Takeoka, "Measurements of acoustic impedance of porous materials using a parametric loudspeaker with phononic crystals and phase-cancellation method," *Appl. Acoust.* **152**, 54–62 (2019).
⁶A. Romanova, K. V. Horoshenkov, and A. Hurrell, "An application of a parametric transducer to measure acoustic absorption of a living green wall," *Appl. Acoust.* **145**, 89–97 (2019).
⁷V. F. Humphrey, "The measurement of acoustic properties of limited size panels by use of a parametric source," *J. Sound Vib.* **98**(1), 67–81 (1985).
⁸V. F. Humphrey, S. P. Robinson, J. D. Smith, M. J. Martin, G. A. Beamish, G. Hayman, and N. L. Carroll, "Acoustic characterization of panel materials under simulated ocean conditions using a parametric array source," *J. Acoust. Soc. Am.* **124**(2), 803–814 (2008).
⁹K. Tanaka, C. Shi, and Y. Kajikawa, "Binaural active noise control using parametric array loudspeakers," *Appl. Acoust.* **116**, 170–176 (2017).
¹⁰M. F. Hamilton and D. T. Blackstock, *Nonlinear Acoustics* (Acoustical Society of America, Melville, NY, 2008).
¹¹M. Červenka and M. Bednářík, "Non-paraxial model for a parametric acoustic array," *J. Acoust. Soc. Am.* **134**(2), 933–938 (2013).
¹²T. Muir, L. Mellenbruch, and J. Lockwood, "Reflection of finite-amplitude waves in a parametric array," *J. Acoust. Soc. Am.* **62**(2), 271–276 (1977).
¹³G. S. Garrett, J. N. Tjøtta, R. L. Rolleigh, and S. Tjøtta, "Reflection of parametric radiation from a finite planar target," *J. Acoust. Soc. Am.* **75**(5), 1462–1472 (1984).
¹⁴L. S. Wang, B. V. Smith, and R. Coates, "The secondary field of a parametric source following interaction with sea surface," *J. Acoust. Soc. Am.* **105**(6), 3108–3114 (1999).
¹⁵F. J. Pompei, "Sound from ultrasound: The parametric array as an audible sound source," Ph.D. dissertation, Massachusetts Institute of Technology, Cambridge, MA, 2002, available at <https://dspace.mit.edu/handle/1721.1/7987>.
¹⁶J. Zhong, R. Kirby, and X. Qiu, "A spherical expansion for audio sounds generated by a circular parametric array loudspeaker," *J. Acoust. Soc. Am.* **147**(5), 3502–3510 (2020).
¹⁷M. Arnela, O. Guasch, P. Sánchez-Martín, J. Camps, R. Alsina-Pagès, and C. Martínez-Suquía, "Construction of an omnidirectional parametric loudspeaker consisting in a spherical distribution of ultrasound transducers," *Sensors* **18**(12), 4317 (2018).
¹⁸H. E. Bass, L. C. Sutherland, and A. J. Zuckerwar, "Atmospheric absorption of sound: Update," *J. Acoust. Soc. Am.* **88**(4), 2019–2021 (1990).
¹⁹H. E. Bass, L. C. Sutherland, A. J. Zuckerwar, D. T. Blackstock, and D. M. Hester, "Atmospheric absorption of sound: Further developments," *J. Acoust. Soc. Am.* **97**(1), 680–683 (1995).
²⁰S. I. Aanonsen, T. Barkve, J. N. Tjøtta, and S. Tjøtta, "Distortion and harmonic generation in the nearfield of a finite amplitude sound beam," *J. Acoust. Soc. Am.* **75**(3), 749–768 (1984).
²¹M. Červenka and M. Bednářík, "A versatile computational approach for the numerical modelling of parametric acoustic array," *J. Acoust. Soc. Am.* **146**(4), 2163–2169 (2019).
²²J. Zhong, R. Kirby, and X. Qiu, "A non-paraxial model for the audio sound behind a non-baffled parametric array loudspeaker (L)," *J. Acoust. Soc. Am.* **147**(3), 1577–1580 (2020).
²³I. Rudnick, "The propagation of an acoustic wave along a boundary," *J. Acoust. Soc. Am.* **19**(2), 348–356 (1947).
²⁴ISO 9613-1:1993. "Acoustics—Attenuation of sound during propagation outdoors—Part 1: Calculation of the absorption of sound by the atmosphere" (International Organization for Standardization, Geneva, Switzerland, 1993).
²⁵P. F. Davis and P. Rabinowitz, *Methods of Numerical Integration* (Academic, San Diego, CA, 1984).
²⁶Z. Tu, J. Lu, and X. Qiu, "Robustness of a compact endfire personal audio system against scattering effects (L)," *J. Acoust. Soc. Am.* **140**(4), 2720–2724 (2016).
²⁷P. Ji and J. Yang, "An experimental investigation about parameters' effects on spurious sound in parametric loudspeaker," *Appl. Acoust.* **148**, 67–74 (2019).
²⁸ISO 10534-2:2001, "Acoustics—Determination of sound absorption coefficient and impedance in impedance tubes—Part 2: Transfer-function method" (International Organization for Standardization, Geneva, Switzerland, 2001).